PCCP

H-bonding Structures of 1-Ethyl-3-methylimidazolium Trifluoroacetate: A Vibrational Spectroscopic Study

Journal:	*Physical Chemistry Chemical Physics*
Manuscript ID	CP-ART-03-2025-000819
Article Type:	Paper
Date Submitted by the Author:	01-Mar-2025
Complete List of Authors:	Mukherjee, Kallol; University of Pittsburgh Hall, Sarah; Colorado State University, Chemistry Krummel, Amber; Colorado State University, Chemistry

H-bonding Structures of 1-Ethyl-3-methylimidazolium Trifluoroacetate: A Vibrational Spectroscopic Study

Kallol Mukherjee, Sarah Hall and Amber Krummel*

Department of Chemistry, Colorado State University, Fort Collins, CO 80523

We have investigated the H-bonding structure of the ionic liquid (IL) 1-ethyl-3-methylimidazolium trifluoroacetate ([Emim:TFA]) via linear and two-dimensional infrared (2DIR) spectroscopy. We directly probed the asymmetric carbonyl stretching mode of the trifluoroacetate anion rather than using an extrinsic solute molecule as a vibrational probe, the more common approach in 2DIR studies of ILs. The C=O asymmetric stretching mode exhibits multimodal character in both linear IR and 2DIR measurements, indicating structural inhomogeneity in the H-bonding of TFA. Solvent-dependent linear IR spectra of dilute Emim:TFA in two protic (D_2O and MeOH-d4) and two aprotic (DMSO-d6 and acetonitrile) solvents, comparisons with NaTFA spectra in these same solvents, and DFT calculations of Emim:TFA and small, solvated ion clusters were used to characterize the H-bonding structures present in the neat ionic liquid. The most prominent IR feature near 1690 cm^{-1} originates from hydrogen bonding between TFA and the C2H and C4/5H imidazolium ring protons. Calculations of the two different types of H-bonding interactions, C2H (and C6H, C7H)-TFA and C4H (and/or C5H)-TFA, indicate that their frequencies are different by several wavenumbers. Higher frequency features (>1695 cm^{-1}) are associated with thosetriple ion structures and higher aggregates where the TFA makes a weak hydrogen bond to $Emim^+$. The appearance of cross-peak features in the time-zero 2DIR spectra indicates the presence of intermolecular coupling between the C=O stretching modes of TFA anions, which can be expected for such pure IL systems. When diluted in polar aprotic solvents, Emim:TFA exists predominantly in ion pairs, while in polar protic solvents solvent-separated ions are the dominant species. The existence of significant ionic aggregation is only visible in the neat ionic liquid.

I. Introduction: Over the past few decades, ionic liquids (ILs) have received considerable attention as potential replacements for conventional organic solvents. Easy tunability of their thermophysical properties via cation and/or anion variation together with low vapor pressures and high thermal stabilities are among the most attractive features of ionic liquids compared to common organic solvents. Their application in energy storage and conversion devices,[1–3] the pharmaceutical industry,[4–6] as carbon capture materials[7,8] and as solvent media for chemical synthesis[9–11] is rapidly advancing. Understanding the solution structure and dynamics of ionic liquids is fundamental to making their use in such applications more efficient and effective. Hydrogen bonding interactions play a key role in determining the structure and dynamics of most ionic liquids.[12–14] Because this hydrogen bonding usually occurs between cations and anions, it is sometimes called 'doubly ionic H-bonding', and it is considered different than H-bonding between uncharged species.[12,14] The strength of this interaction can be tuned by varying either the cation or the anion, which enables tuning of many structural and dynamic properties of the medium. In the present study we investigate the H-bonding structure of the ionic liquid 1-ethyl-3-methylimidazolium trifluoroacetate (Emim:TFA) using linear and nonlinear vibrational spectroscopy and DFT calculations of small ionic clusters.

Part of our motivation for studying Emim:TFA is based on two important observations from recent work. First, acetate-based ionic liquids appear to be good candidates for CO_2 absorption in carbon capture and storage (CCS) applications.[15–18] In addition, Emim:TFA (and its aqueous mixtures) are finding applications in the electrochemical reduction of CO_2.[19] The drastic difference between the CO_2 absorption efficiencies of Emim:TFA and Emim acetate [16] needs further investigation, as may provide insights needed to improve the performance of ILs in CCS. The TFA anion is also among the most basic of common IL anions. Because the basicity of the anion is thought to play a crucial role in the absorption of many gases in ionic liquids,[12,20,21] investigating H-bonding within Emim:TFA is of interest beyond the CCS field.

A previous study[22] on binary mixtures of 1-butyl-3-methylimidazolium trifluoroacetate (Bmim;TFA) and two protic solvents, water and methanol, pointed out how the H-bonding interactions of Bmim;TFA vary with cosolvent identity and concentration and suggested the dominant H-bonding interactions present in different concentration regimes. However, that study

did not discuss the H-bonding interactions of the neat ionic liquid in detail. The questions remaining to be answered are: 1) How heterogeneous (or homogeneous) is the H-bonding structure of neat Emim:TFA? 2) How different are the C(2)H…anion and C(4/5)H…anion H-bonding interactions? 3) Is there any vibrational coupling between the differently H-bonded species? In this work we primarily concentrate on the H-bonding structure of the ionic liquid by exploiting the asymmetric carbonyl stretching mode of the TFA anion.

Vibrational spectroscopy is one of the most heavily practiced approaches to investigating H-bonding interactions in liquids. Over the past 20 years, both linear and nonlinear vibrational spectroscopic methods have been extensively employed to explore both the H-bond structure and the dynamics of ionic liquids.[23–29] 2DIR spectroscopy is one of the very few techniques that enables simultaneous probing of structure and dynamics on ultrafast timescales. For this reason 2DIR spectroscopy is finding numerous applications in a wide range of research areas, such as the biological sciences,[30–34] electrochemistry and energy storage,[35–37] gas absorption chemistry,[38–40] and photochemistry.[41–43] Application of 2DIR spectroscopy has been successfully used to explore numerous ionic liquids since the beginning of the current century.[25,44–48] In most such studies extrinsic vibrational probes, for example the thiocyanate anion, various metal carbonyls, and water have been employed to name a few.[23,44,46,49–53] The disadvantage of this method is that the information obtained depends on the probe selected. Furthermore, some details of the neat liquid, for example the importance of intermolecular coupling between oscillators, cannot be accessed in such experiments. In the present work we choose to directly probe the neat ionic liquid using the asymmetric carboxylate stretch of TFA anion, circumventing the problem of high absorptivities by monitoring thin films of the neat liquid.

We present a detailed dissection of the asymmetric carboxylate stretch of the TFA anion in neat Emim:TFA, including initial observations of the time-zero 2DIR spectrum of this liquid. Dilute solution spectra and electronic structure calculations, used to help interpret the complex band shape observed in the neat liquid, are also reported. 2DIR studies of the dynamics probed by the TFA asymmetric stretch will be reported in a future contribution.

II. Materials and Sample Preparation: 1-Ethyl-3-methylimidazolium trifluoroacetate ([Emim:TFA], > 97%) and sodium trifluroacetate (NaTFA, 99.4%) were purchased from Iolitec and AmBeed Chemicals, respectively. They were used as received. The solvents deuterium oxide

(D_2O, Cambridge Isotope Laboratory, 99.9%), deuterated dimethyl sulfoxide (DMSO-d6, Aldrich, 99.9%), acetonitrile (MeCN, Oakwood Chemicals, 99%) and deuterated methanol (MeOH-d4, Aldrich, 99%) were also used as received. For sample preparation, the required amount of ionic liquid (or NaTFA) was added to each solvent to achieve a concentration of ionic liquid (or NaTFA) $\leq$ 0.1 mole fraction (MF onwards). Hydrophilic ionic liquids like [Emim:TFA] contain some amount of residual water even after thorough drying. It is well established that water can have a profound impact on the structure and dynamics of ionic liquids.[54–61] As such, it is important to monitor the water content in the ILs. A detailed discussion on the water content and its structure in the [Emim:TFA] samples is presented in Section A of the Supporting Information.

III. Methods:

A. Linear IR measurements and analysis: Linear IR spectra were recorded at 2 cm^{-1} resolution using a Bruker Vertex 70v spectrometer. Samples were placed between two 2-mmthick, 25 mm diameter CaF_2 windows. Linear IR spectra of pure [Emim:TFA] were recorded without incorporating any spacers between the two windows in order to maintain the optical density < 1.0. The water content of [Emim:TFA] in the spectroscopic samples was found to be ~ 0.2 MF, based on the intensity of the OH stretching band of water (3200 - 3800 cm^{-1}). Linear IR spectra were fitted using multi-Voigt (or multi-Gaussian) fitting models in both Origin and MATLAB software.

B. 2DIR measurements and analysis: The pure ionic liquid sample was subjected to 2DIR spectroscopy. In this technique three mid-IR pulses interact with the sample in a controlled way to generate a third order signal. The 2DIR spectrometer used in these experiments has been described in detail elsewhere.[62,63] Briefly, output pulses (~50 fs, ~2.7 W, centered at 785 nm) from a regenerative chirped pulse amplifier (Wyvern 1000, KM Laboratories), seeded with a Ti:sapphire oscillator, were directed to an optical parametric amplifier (TOPAS prime) having a difference frequency generation stage ($AgGaS_2$) that produced tunable mid-IR light. Thus-generated mid-IR pulses, centered at 6000 nm, and having ~ 10μJ energies, were then directed to a 90:10 beam splitter. Most of the IR light was passed through a mid-IR pulse shaper (Ge-AOM, Isomet Corporation LS600-1109) to generate phase-stable pulse pairs with a controllable time delay, τ, between the pulse pairs. The τ time delay was scanned out to 6 ps using 15 femtosecond step sizes. The probe light was directed to the sample by passing it through a computer-controlled delay stage, generating a time delay (T_w) between the second and third pulses. Both the pump and probe beams

were spatially and temporally overlapped at the sample to generate the third order signal. A four-frame phase cycling scheme and a partially rotating frame (1400 cm^{-1}) was used to eliminate the unwanted transient absorption and pump scatter contributions from the 2D IR spectra. In the absence of the sample, the energy of the pump and probe pulses were approximately matched to each other at the detector. After the sample, the probe beam was recollimated and directed to a 64-element mercury cadmium telluride (MCT) array detector. T_w was scanned from 0 ps to 2 ps during the 2D IR measurements; the spectra presented in this work have a T_w = 0.2 ps. The spectrometer box was purged with dry air and the analysis of the 2DIR data was carried out using codes written in MATLAB. All linear IR and 2DIR measurements were carried out at room temperature, 21 ± 1 °C.

C. Electronic structure calculations: Density functional theory (DFT) calculations of small clusters of ionic liquid with and without the addition of dipolar solvent molecules were carried out using the Gaussian16 [64] suite of programs. In the case of purely ionic clusters, individual ions were first geometry optimized and then combined into ion pairs or aggregates before being reoptimized. For clusters including dipolar solvent molecules, pre-optimized ions/ion pairs and solvent molecules were combined according to earlier reports on their coordination and then subjected to complete geometry optimization. For example, to model TFA^- in D_2O we first took the optimized TFA^- anion and added four pre-optimized water molecules corresponding to the reported hydration number of TFA^- anion,[65] and then optimized this structure. Similar calculations of ionic liquids and solvated ion clusters[22,66–71] have been used to successfully interpret experimental vibrational spectra of ILs. Final optimizations and calculations of vibrational frequencies employed the B3LYP functional, the 6-31++G(d,p) basis set and implicit solvation using the conductor-like polarizable continuum model (CPCM). The basis set and the functional were selected based on previous reports. [66–71] Frequency analysis showed all the structures reported here correspond to local minima in the potential energy surface. No scaling factor was applied to the calculated frequencies reported.

IV. Results and discussion:

A. The asymmetric carbonyl stretch band of TFA^- in neat [Emim:TFA]:

A1. Linear IR measurements: Figure 1 represents the linear IR spectra of the asymmetric carbonyl stretching mode of Emim:TFA and the corresponding multi-Voigt fit. Spectra reported

in prior studies[22,67] of similar imidazolium TFA ionic liquids agree well with this spectrum, however no decomposition of the band shape has previously been attempted. The spectrum in this region consists of a primary peak near 1690 cm^{-1} and a shoulder peak at a lower frequency. The primary peak is not well fit to a single component having a simple shape. After trying a variety of fitting models, including multi-Gaussian and multi-Lorentzian fits, based on both the fit quality and the consistency of the parameters provided, the unconstrained 3-component Voigt fit shown in figure 1 was chosen as the best representation. It is important to note, that independent of the lineshape chosen, at least three components were needed to adequately represent the 1640 -1740 cm^{-1} region of the linear IR spectrum. (See figure S1.) Examination of the second derivative of the spectrum in this region provided additional support for needing three components. We assign all features in this region to the asymmetric stretch of TFA in three types of hydrogen bonding environments. The two subcomponents of the primary peak are attributed to environments of the neat ionic liquid, whereas the much broader band centered at 1672 cm^{-1} is attributed to TFA interacting with trace water present that could not be removed from the sample. Please see Section A, which includes figure S2 and table S3, of the Supporting Information for further details on trace water. The 1688 cm^{-1} component of the primary band is assigned to TFA:Emim contact ion-pairs minimally affected by interactions with other ions, and the 1697 cm^{-1} component we assign to TFA anions involved in ionic aggregates. The reasons behind these peak assignments are presented in the following sections.

A2. 2DIR measurements: Figure 2 compares the 2DIR spectrum of Emim:TFA to the linear spectrum. The 2DIR data shown here were collected in a co-polarization geometry. Figure S4 shows the corresponding cross-polarized spectrum. In either polarization, the 2D spectrum of the TFA asymmetric stretch is complex, consisting of three negative peaks along the diagonal, which strongly supports the use of three peaks to fit the linear spectrum.

Several cross-peak features are also observed in the 2DIR spectra shown in Figs. 2 and S4. Figures 3 and S5 depict representative pump slices at three different pump frequencies (ω_1=1698 cm^{-1}, ω_1= 1687 cm^{-1} and ω_1= 1679 cm^{-1}) of the co-polarized 2DIR spectra taken at different T_w values; these slices are used to distinguish between the diagonal peak pairs and cross peak pairs. The details are provided in section B of the Supporting Information. The cross peaks indicate intermolecular coupling between the IL molecules and they are expected for such condensed phase neat systems.

From the displacement between positive and negative features of the diagonal peaks estimates of ~ 18 cm^{-1} to ~ 24 cm^{-1} are obtained for the diagonal anharmonicity of each species. Such values are consistent with anharmonicities of the asymmetric stretch reported in other TFA systems.[72–74] (See section B of the Supporting Information for more details.) A value of 25 cm^{-1} is also obtained from gas-phase DFT calculations of an isolated TFA anion. We do not consider the T_w dependence of the 2DIR spectra further in this work. Here we use the 2DIR spectra mainly to emphasize the multimodal nature of this band of neat Emim:TFA. Next, we consider linear IR measurements of Emim:TFA diluted in other solvents in order to understand the origin of the structures present in the liquid.

B. Linear IR spectroscopy of diluted TFA^- solutions: In Figure 4 we compare the neat spectrum (Fig. 4a) to spectra of dilute Emim:TFA (mole fraction ~0.1) in the aprotic solvents acetonitrile and dimethylsulfoxide (DMSO-d6) and in the protic solvents D_2O and methanol-d4 (Fig. 4b). Figure 4c presents analogous spectra of NaTFA solutions. In the dilute solutions shown here, the TFA stretching bands of Emim:TFA and NaTFA show features at frequencies similar to those extracted from fits of the neat Emim:TFA spectra. Representative fits of some of these solution spectra are illustrated in Figs. S6-S7 and component frequencies and amplitudes of all spectra are summarized in table S8.

Consider first the spectra of dilute NaTFA shown in Fig. 4c, as these spectra exhibit the most dramatic variations with solvent. The spectrum of NaTFA in D_2O consists of a single peak near 1674 cm^{-1}, in agreement with earlier reports.[72,73] (See also Fig. S6.) A similarly simple spectrum is found for NaTFA in the aprotic solvent DMSO-d6, but in this case the peak occurs at a much higher frequency, ~1690 cm^{-1} and this is also consistent with earlier reports.[73] The same mode in acetonitrile also has a peak near 1690 cm^{-1} but it is remarkable in its breadth, having nearly three times the width of the NaTFA/DMSO spectrum. As shown in Fig. S7, at least four components are required to achieve a good fit to this broad asymmetric band. Finally, in methanol-d4 the NaTFA spectrum peaks near to the spectrum in D_2O, however in methanol the spectrum is asymmetric in a manner that suggests the presence of an additional components at higher frequencies.

The dilute-solution spectra of Emim:TFA (Fig. 4b) display both similarities and dissimilarities to the NaTFA spectra. In D_2O, the Emim:TFA spectrum peaks at a very similar frequency to the

NaTFA/D_2O spectrum, but the Emim:TFA spectrum exhibits a distinct shoulder at higher frequencies (Fig. S6). The spectrum of dilute Emim:TFA in methanol-d4 is also very similar to that of NaTFA, except that the contribution of the secondary peak on the high frequency side increases compared to NaTFA, see Table S8.

All of the aforementioned observations can be reasonably explained in the following way. As these two salts share a common anion, differences in their IR spectra must arise from differences in how their cations interact with TFA and surrounding solvent. Let's again start with D_2O as the solvent. Both TFA^- and Na^+ are well solvated by D_2O, as they are a strong base and a strong acid, respectively. It is therefore reasonable to attribute the sole peak at 1674 cm^{-1} in NaTFA/D_2O to TFA^- fully solvated by D_2O. Similarly, in the [Emim:TFA]/D_2O system, the primary peak found at 1675 cm^{-1} is assigned to fully solvated TFA^-. The presence of a secondary peak near 1690 cm^{-1} in the [Emim:TFA]/D_2O mixture can be rationalized by the differences expected for solvation of $Emim^+$ compared to Na^+ in water. Based on the close proximity of this secondary peak to the primary peak of neat Emim:TFA (~1688 cm^{-1}) and several earlier reports[75–77] which suggest existence of ion pairs in diluted (aqueous) Emim-based ionic liquid systems, we attribute this 1690 cm^{-1} peak to Emim:TFA ion pairs. Whereas Na^+ is expected to be strongly solvated by water, the much weaker interactions between $Emim^+$ and water encourage greater Emim - TFA ion pairing than in NaTFA, where such paring is negligible. The same difference is observable in the other protic solvent, methanol-d4, where the contribution of the secondary peak increases from NaTFA to Emim:TFA.

Next, we move to the DMSO-d6 solvent, which is an excellent electron pair donor but poor electron pair acceptor.[78] Being a weak acceptor,[78] the DMSO is expected to poorly solvate the TFA anion. For this reason, ion pairing is expected to be favored in DMSO and we therefore assign the predominant ~1690 cm^{-1} peak observed for both Emim:TFA and NaTFA in DMSO, to contact ion pairs. The nearly identical frequencies of the TFA stretch ion paired to two markedly different cations in the same solvent may seem surprising. But one should keep in mind that the solvation of the $Emim^+$:TFA^- and Na^+:TFA^- ion pairs is expected to be significantly different. In DMSO solution Na^+ is expected to be strongly coordinated to two or more DMSO molecules in addition to the TFA anion. As shown by the calculations in the following section, this coordination leads to significant modification of the TFA stretch in Na^+:TFA^-. In contrast, the frequency of

$Emim^+$:TFA^- is little perturbed by solvation in such aprotic solvents, resulting in the frequencies of the two ion pairs being nearly the same.

The differences between NaTFA and Emim:TFA are most pronounced in the solvent acetonitrile, which is neither a good electron pair donor or acceptor.[78] Because Na^+ is only weakly coordinated by acetonitrile, not only ion pairs but also higher order ionic aggregates such as triple ions, are expected in NaTFA/acetonitrile solutions. This mix of species is manifested by the extremely broad spectrum in acetonitrile (figure 4 and S7). We note that the spectrum of NaTFA in DMSO is less symmetric than the spectrum of [Emim:TFA]/DMSO, suggesting that some limited higher-order ionic aggregates may also be present even in DMSO.

The assignments made here differ from those proposed in an early study of LiTFA and tetrabutylammoniumTFA in DMSO and acetonitrile.[79] That study ascribed the ~1690 cm^{-1} peak to free TFA^- anions and the higher frequency features of the spectra to ion pairs and ionic aggregates. Because we find a similar peak near 1690 cm^{-1} in both the ionic liquid Emim:TFA and solid NaTFA,[80,81] we believe it is more reasonable to attribute this peak to contact ion pairs than to free TFA, despite the fact that such a peak also occurs when TFA salts are diluted in DMSO. Observation of this peak when Emim:TFA and NaTFA are diluted in protic solvents such as water and methanol, where any unpaired TFA^- would be expected to be hydrogen bonded rather than free, also supports our interpretation. In the following section we use DFT calculations to examine the possible origins of this band and provide further support for the above assignments.

C. DFT calculations of ions, ion pairs and ionic aggregates: Similar to prior studies,[22,66,67,82] we first performed calculations on single and double ion pairs. Figure 5 shows the optimized structures of two different types of single ion pairs and a double ion pair. To mimic the effects of longer-range interactions with the surrounding liquid, these calculations were performed in an implicit solvent environment of dielectric constant ~ 27, the value reported for Emim:TFA.[83]

Before using these calculations to interpret the experimental spectra, we first discuss the reliability of such calculations. First, we note that the results in figure 5 agree closely with similar calculations[22,67] of single and double ion pairs of 1-butyl-3-methylimidazolium trifluoroacetate (Bmim:TFA). Further validation comes from calculations of [Emim:TFA]/D_2O mixtures, where we can compare the observed concentration dependence of both the TFA^- band and the aromatic C-H stretching bands with corresponding calculations. Experimentally we see a continuous red

shift for the carbonyl stretching mode and a systematic blue shift of the C2H stretching frequency with the addition of D_2O (see figure S11). Figure S10 presents the changes in the optimized structure of the ion pair with the addition of water molecules around it and the changes in the frequency values show a nice agreement with the experimental observation. It is noteworthy that with increasing D_2O concentration we see experimentally the appearance of a double peak character in the C2H stretching mode (~ 3090 cm^{-1}), shown in figure S11, which corroborates well with the bimodal nature of the asymmetric carbonyl stretching mode at high D_2O concentration. We suspect that this bimodal character of both the modes at high D_2O concentration reflects the existence of two types of TFA solvates: the $Emim^+$:TFA^- ion pairs and D_2O-solvated TFA anions. Similar blue shifts of the C2H stretching mode have also been reported for various $Bmim^+$ ionic liquids with addition of D_2O.[84] Note that to perform the calculation for TFA^- completely solvated by water we use four explicit water molecules based on the reported hydration number of TFA anion in aqueous solution,[65] surrounded by an implicit water milieu. Not only the blue shift of the C2H frequency but also the experimentally observed blue shift of the C4/5H stretching frequency (figure S11) is well captured in our DFT calculations (not presented here). These observations validate the calculation method employed here is suitable for interpreting the infrared spectra of the pure ionic liquid and its mixtures with dipolar solvents.

Now we return to calculations of ion pairs and higher ionic aggregates mixed with dipolar solvents. TFA^- carboxylate and $Emim^+$ C2H stretching frequencies of both Emim:TFA and NaTFA are summarized in Table S9. As shown by these calculations in the gas phase, ion pairing causes a substantial red shift of the asymmetric carbonyl stretch, a shift of -45 cm^{-1} when paired with $Emim^+$ and -86 cm^{-1} paired with Na^+. However, when explicit DMSO or acetonitrile are included to complete solvation of Na^+, the TFA^- asymmetric stretch frequencies of Na^+:TFA^- and $Emim^+$:TFA^- are much closer in frequency (8 cm^{-1} in acetonitrile), which is consistent with the small differences observed experimentally (Table S8).

The calculated frequencies of the TFA^- stretch obtained from the C2H---TFA and C4/5H---TFA H-bonding configurations, presented in figure 5(a), are ~1701 cm^{-1} and ~1704 cm^{-1}, respectively. Similarly small differences of 3 - 4 cm^{-1} are calculated for other configurations, including those containing two ion pairs. This variation is much smaller than the 9-10 cm^{-1} difference between the two components needed to fit the primary TFA peak (1690/1700 cm^{-1}) in the linear spectra of

bulk and dilute Emim:TFA (Table S8) and the distinct diagonal peaks found in the 2DIR spectrum (Fig. 2). Calculations of triple ion clusters ($Emim_1TFA_2^-$) such as that shown in Fig. S12 produce components at higher frequencies than ion pairs and component splitting of ~8 cm^{-1}. We therefore propose that the lower frequency component observed near 1690 cm^{-1} reflects TFA^- in $Emim^+$:TFA^- pairs in which it is well hydrogen bonded to a single $Emim^+$ cation, at any of the three aromatic hydrogen atoms. In contrast, the higher frequency component near 1700 cm^{-1} is proposed to reflect TFA^- in configurations such as the triple-ion example in Fig. S12, wherein it makes only a weak hydrogen bond to $Emim^+$. The closest carboxylate oxygen…. hydrogen interactions, which have the following order: C2H…carbonyl (~ 1.96 Å, in ion pairs and ionic aggregates) > C4/5H…carbonyl (~ 2.05 Å in ion pairs) > C4/5H…carbonyl (~ 2.13 Å in ionic aggregates), also indicates the presence of weakest H-bonding in ionic aggregates. The weaker the H-bonding interaction the higher is the asymmetric carboxylate stretching frequency of TFA^-. This interpretation is consistent with the relative areas of the 1690 and 1700 peaks in neat Emim:TFA and in dilute solution in DMSO and acetonitrile (Table S8); species with weak hydrogen bonding get solvated more easily with dilution than the ones having stronger hydrogen bonding.

Next, we will discuss the possible origin of the observed cross-peak features in the 2DIR spectra. Visualization of the TFA asymmetric stretch of various ion pair geometries and ionic aggregates such as that shown in Fig. S12, shows that coupling exists between the asymmetric carbonyl stretch of different TFA^- anions. This coupling is quenched upon substitution of O^{16} with O^{18} in one of the TFA anions. Such coupling should result in cross peaks and give rise to cross-peaks like those observed between the diagonal features at 1687 and 1698 cm^{-1}.

D. Lower frequency components in the 2DIR and linear IR spectra: We finally discuss the feature(s) appearing below 1685 cm^{-1} in both the linear and 2DIR spectra of pure Emim:TFA and some of its dilute solutions. As already mentioned in section IV. A1 we believe that the 1679 cm^{-1} band can be attributed to water impurities interacting with the TFA anion. However, another possibility is that the ω_1= 1679 cm^{-1} band is a cross-peak feature arising due to the strong diagonal feature at ω_1= 1687 cm^{-1} and an obscured diagonal peak at $\omega_1 \approx$ 1679 cm^{-1}. This obscured diagonal feature near 1679 cm^{-1} can be related to water-solvated TFA anions or to an overtone or combination band of the ion pairs or triple ions. Anharmonic calculations of isolated TFA^- indicate a moderately intense vibration (a combination band between the symmetric CF_3 stretching mode

and a lower frequency CF_3 bending mode) exists ~20 cm^{-1} below the asymmetric stretch. We think this value is much higher than what we see in the experiment. Although, to make a better comparison one should run similar calculations with the ion pairs (or triple ions). Based on the following observations we assigned this peak to the water-solvated TFA anions: : 1) Our DFT calculations and water concentration dependent linear IR experiments, presented in figure S10 and S11, shows that with addition of water molecules the asymmetric carboxylate stretch undergoes a continuous red shift and from our NMR experiments we see the presence of water impurities in the medium, 2) our preliminary experiments in which we dope water in a dilute solution of Emim:TFA in acetonitrile indicate that a band at ~1680 cm^{-1} band appears at low doping and it shifts to lower frequencies and intensifies with further water addition, and 3) with dilution, irrespective of the solvent medium, the contribution of this feature to the linear spectra diminishes (see table S8). While the origin of these features seems partly clear, some questions remain to be addressed. For example, in the 2DIR spectrum why is the negative feature near 1679 cm^{-1} (ω_1) displaced from the diagonal and what is the origin of the positive peak (an excited-state absorption) around 1675 cm^{-1}? Such displacement of the diagonal feature can be caused by interference between ground and excited state transitions.[85] Further 2DIR measurements are currently underway to help understanding these observations and make more definitive assignment of the aforementioned low-frequency features.

It should also be mentioned that a band between 1640 - 1670 cm^{-1} is observed in the linear spectra of diluted Emim:TFA in different solvents (Table S8). Such bands originate from the bending mode of the residual H_2O present in Emim:TFA (and in other solvents) while in D_2O this contribution arises from a broad D_2O combination band (~1590 cm^{-1} [86]). It is noteworthy that this region of the spectra contains contributions from both water-TFA and water-solvent, e.g. water-DMSO-d6, types of interactions, and as a result we get a cumulative response in the deconvoluted spectra.

V. Concluding remarks: We have used linear IR and 2DIR spectroscopy together with DFT calculations of the TFA carboxylate asymmetric stretch of Emim:TFA in the neat ionic liquid and in association with other solvents. By focusing on the carboxylate asymmetric stretch of the TFA anion as an intrinsic IR probe, we have been able to elucidate the various types of hydrogen bonding in which TFA^- participates. In most solvents the vibrational spectrum of the carboxylate

asymmetric stretch of TFA^- is complex, most often requiring at least three components to adequately represent the observed spectrum. We attribute these components, common to neat Emim:TFA as well as to TFA^- in dilute solution, to four types of solvation structures in which this anion is found. The structures give rise to components in slightly different frequency ranges, as summarized in Figure 6. In neat Emim:TFA, the dominant spectral features are observed between 1688-1710 cm^{-1}, which we attribute to TFA^- hydrogen bonded to $Emim^+$ primarily through its aromatic ring hydrogen atoms (Fig. 5) in ion pairs as well as less well-defined ionic aggregates. In dilute mixtures with polar aprotic solvents like DMSO and acetonitrile, TFA^- exists primarily ion paired with its counterion, as indicated by a dominant band in this same spectral region. Comparisons between Emim:TFA and NaTFA solutions as well as DFT calculations show the TFA^- spectrum can be surprisingly insensitive to the identity of the cation in some solvents, and that this insensitivity depends upon cation – solvent interactions. In solvents with little electron donating ability like acetonitrile, aggregation of NaTFA leads to some of the broadest TFA^- spectra observed. In protic solvents like water and methanol, depending on the identity of the cation, hydrogen bonding with solvent competes with ion pairing, which leads to components at lower frequencies (1674-1680 cm^{-1}). Finally, because of the difficulty of completely removing water from hydroscopic compounds containing TFA^-, expect some portions of the lowest frequency components are due to TFA^- hydrogen bonding to residual water.

By directly observing the TFA^- carboxylate asymmetric stretch with 2DIR in Emim:TFA, we have found that intermolecular coupling occurs in the neat ionic liquid. Preliminary 2DIR experiments on Emim:TFA in solvents such as acetonitrile show this coupling decreases with dilution. In future work we will describe the dynamics of the diagonal and cross peak features of the 2DIR spectra, as well as probing the solvent dependent dynamics of ion pairs.

Data Availability: The data supporting this article have been included as part of the Supplementary Information.

Supplementary Information: Visit the 'Supplementary Information (link)' for Water content and structure in Emim:TFA, two-Voigt deconvolution of the asymmetric stretching mode of undoped Emim:TFA, comparison between the residuals of two-Voigt and three-Voigt fits of the asymmetric stretching mode of undoped Emim:TFA, decomposition of the OH stretching regime of water, Tabulated comparison between the peak frequencies obtained from our fit and estimated peak

frequencies form literature, time-zero 2DIR spectra of undoped Emim:TFA in two different polarization, anharmonicity of the 1683 cm^{-1} (along the pump axis) feature of 2DIR spectra of pure Emim:TFA, deconvolution of linear IR spectra of NaTFA and Emim:TFA in D_2O and acetonitrile, tabulated fit parameters of solvent dependent linear IR spectra of NaTFA and Emim:TFA along with the pure Emim:TFA, tabulated calculated frequency values for different Emim:TFA and NaTFA ion pairs using different calculation methods, optimized structures of two different single ion pairs and one double ion pair, effect of water addition in a representative ion pair, water concentration dependent C-H and asymmetric carbonyl stretching spectra of [Emim:TFA]/Water system, representative optimized structure of a triple ion of undoped Emim:TFA, linear IR spectra of asymmetric carbonyl stretching band for diluted Emim:TFA in dipolar solvent, acetonitrile, and ionic liquid Emim:NTF_2.

Acknowledgements: The authors would like to thank the Molecular Dynamics and Theoretical Chemistry Program in the Air Force Office of Scientific Research for the full support of this project (Award #FA9550-20-1-0401). KM acknowledges the generous support of Professor Mark Maroncelli (Department of Chemistry, Penn State University, USA) in electronic structure calculations.

References:

1. M. Watanabe, M. L. Thomas, S. Zhang, K. Ueno, T. Yasuda and K. Dokko, *Chem. Rev.*, 2017, **117**, 7190–7239.

2. T. Tsuda and C. L. Hussey, *Electrochem. Soc. Interface*, 2007, **16**, 42–49.

3. K. Karuppasamy, J. Theerthagiri, D. Vikraman, C.-J. Yim, S. Hussain, R. Sharma, T. Maiyalagan, J. Qin and H.-S. Kim, *Polymers*, 2020, **12**, 918.

4. K. S. Egorova, E. G. Gordeev and V. P. Ananikov, *Chem. Rev.*, 2017, **117**, 7132–7189.

5. I. M. Marrucho, L. C. Branco and L. P. N. Rebelo, *Annu. Rev. Chem. Biomol. Eng.*, 2014, **5**, 527–546.

6. S. N. Pedro, C. S. R. Freire, A. J. D. Silvestre and M. G. Freire, *IJMS*, 2020, **21**, 8298.

7. W. Faisal Elmobarak, F. Almomani, M. Tawalbeh, A. Al-Othman, R. Martis and K. Rasool, *Fuel*, 2023, **344**, 128102.

8. M. Ramdin, T. W. De Loos and T. J. H. Vlugt, *Ind. Eng. Chem. Res.*, 2012, **51**, 8149–8177.

9. A. J. Greer, J. Jacquemin and C. Hardacre, *Molecules*, 2020, **25**, 5207.

10. R. D. Rogers and K. R. Seddon, *Science*, 2003, **302**, 792–793.

11. D. Zhao, M. Wu, Y. Kou and E. Min, *Catalysis Today*, 2002, **74**, 157–189.

12. K. Dong and S. Zhang, *Chemistry A European J*, 2012, **18**, 2748–2761.

13. V. Kempter and B. Kirchner, *Journal of Molecular Structure*, 2010, **972**, 22–34.

14. P. A. Hunt, C. R. Ashworth and R. P. Matthews, *Chem. Soc. Rev.*, 2015, **44**, 1257–1288.

15. A. Yokozeki, M. B. Shiflett, C. P. Junk, L. M. Grieco and T. Foo, *J. Phys. Chem. B*, 2008, **112**, 16654–16663.

16. M. B. Shiflett and A. Yokozeki, *J. Chem. Eng. Data*, 2009, **54**, 108–114.

17. G. Gurau, H. Rodríguez, S. P. Kelley, P. Janiczek, R. S. Kalb and R. D. Rogers, *Angewandte Chemie*, 2011, **123**, 12230–12232.

18. M. Besnard, M. I. Cabaço, F. V. Chávez, N. Pinaud, P. J. Sebastião, J. A. P. Coutinho and Y. Danten, *Chem. Commun.*, 2012, **48**, 1245–1247.

19. J. D. Watkins and A. B. Bocarsly, *ChemSusChem*, 2014, **7**, 284–290.

20. Y. Zhao, M. Pan, X. Kang, W. Tu, H. Gao and X. Zhang, *Chemical Engineering Science*, 2018, **189**, 43–55.

21. B. Lu, Y. Zeng, M. Chen, S. Zhang and D. Yang, *Atmosphere*, 2024, **15**, 229.

22. Q.-G. Zhang, N.-N. Wang, S.-L. Wang and Z.-W. Yu, *J. Phys. Chem. B*, 2011, **115**, 11127–11136.

23. B. Wu, J. P. Breen and M. D. Fayer, *J. Phys. Chem. C*, 2020, **124**, 4179–4189.

24. M. N. Garaga, M. Nayeri and A. Martinelli, *Journal of Molecular Liquids*, 2015, **210**, 169–177.

25. A. Tamimi, H. E. Bailey and M. D. Fayer, *J. Phys. Chem. B*, 2016, **120**, 7488–7501.

26. M. Mohammad Kazemi, M. Namboodiri, P. Donfack, A. Materny, D. Kerlé, B. Rathke and J. Kiefer, *Phys. Chem. Chem. Phys.*, 2017, **19**, 15988–15995.

27. C. S. Santos and S. Baldelli, *J. Phys. Chem. B*, 2009, **113**, 923–933.

28. V. H. Paschoal, L. F. O. Faria and M. C. C. Ribeiro, *Chem. Rev.*, 2017, **117**, 7053–7112.

29. C. Roth, S. Chatzipapadopoulos, D. Kerlé, F. Friedriszik, M. Lütgens, S. Lochbrunner, O. Kühn and R. Ludwig, *New J. Phys.*, 2012, **14**, 105026.

30. Y. S. Kim and R. M. Hochstrasser, *J. Phys. Chem. B*, 2009, **113**, 8231–8251.

31. H. S. Chung, Z. Ganim, K. C. Jones and A. Tokmakoff, *Proc. Natl. Acad. Sci. U.S.A.*, 2007, **104**, 14237–14242.

32. A. L. Serrano, J. P. Lomont, L.-H. Tu, D. P. Raleigh and M. T. Zanni, *J. Am. Chem. Soc.*, 2017, **139**, 16748–16758.

33. C. T. Middleton, P. Marek, P. Cao, C. Chiu, S. Singh, A. M. Woys, J. J. De Pablo, D. P. Raleigh and M. T. Zanni, *Nature Chem*, 2012, **4**, 355–360.

34. I. J. Finkelstein, H. Ishikawa, S. Kim, A. M. Massari and M. D. Fayer, *Proc. Natl. Acad. Sci. U.S.A.*, 2007, **104**, 2637–2642.

35. M. J. Ryan, N. Yang, K. Kwac, K. B. Wilhelm, B. K. Chi, D. J. Weix, M. Cho and M. T. Zanni, *Proc. Natl. Acad. Sci. U.S.A.*, 2023, **120**, e2314998120.

36. J. Lim, K.-K. Lee, C. Liang, K.-H. Park, M. Kim, K. Kwak and M. Cho, *J. Phys. Chem. B*, 2019, **123**, 6651–6663.

37. J. Lim, K. Park, H. Lee, J. Kim, K. Kwak and M. Cho, *J. Am. Chem. Soc.*, 2018, **140**, 15661–15667.

38. J. Y. Shin, S. A. Yamada and M. D. Fayer, *J. Am. Chem. Soc.*, 2017, **139**, 11222–11232.

39. T. Brinzer, E. J. Berquist, Z. Ren, S. Dutta, C. A. Johnson, C. S. Krisher, D. S. Lambrecht and S. Garrett-Roe, *The Journal of Chemical Physics*, 2015, **142**, 212425.

40. T. Brinzer, C. A. Daly, C. Allison, S. Garrett-Roe and S. A. Corcelli, *J. Phys. Chem. B*, 2018, **122**, 8931–8942.

41. N. T. Hunt, *Dalton Trans.*, 2014, **43**, 17578–17589.

42. J. Bredenbeck, J. Helbing and P. Hamm, *J. Am. Chem. Soc.*, 2004, **126**, 990–991.

43. L. M. Kiefer and K. J. Kubarych, *Coordination Chemistry Reviews*, 2018, **372**, 153–178.

44. Z. Ren, T. Brinzer, S. Dutta and S. Garrett-Roe, *J. Phys. Chem. B*, 2015, **119**, 4699–4712.

45. Z. Ren, A. S. Ivanova, D. Couchot-Vore and S. Garrett-Roe, *J. Phys. Chem. Lett.*, 2014, **5**, 1541–1546.

46. A. K. Mora, P. K. Singh and S. Nath, *Journal of Molecular Liquids*, 2022, **358**, 119189.

47. S. A. Yamada, H. E. Bailey, A. Tamimi, C. Li and M. D. Fayer, *J. Am. Chem. Soc.*, 2017, **139**, 2408–2420.

48. B. Guchhait, C. A. Tibbetts, K. M. Tracy, B. M. Luther and A. T. Krummel, *The Journal of Chemical Physics*, 2020, **152**, 164501.

49. L. M. Kiefer and K. J. Kubarych, *J. Phys. Chem. Lett.*, 2016, **7**, 3819–3824.

50. X. Chen, Y. Cui, H. B. Gobeze and D. G. Kuroda, *J. Phys. Chem. B*, 2020, **124**, 4762–4773.

51. M. D. Fayer, D. E. Moilanen, D. Wong, D. E. Rosenfeld, E. E. Fenn and S. Park, *Acc. Chem. Res.*, 2009, **42**, 1210–1219.

52. D. E. Moilanen, D. Wong, D. E. Rosenfeld, E. E. Fenn and M. D. Fayer, *Proc. Natl. Acad. Sci. U.S.A.*, 2009, **106**, 375–380.

53. C. J. Fecko, J. D. Eaves, J. J. Loparo, A. Tokmakoff and P. L. Geissler, *Science*, 2003, **301**, 1698–1702.

54. J. Zhou, X. Liu, S. Zhang, X. Zhang and G. Yu, *AIChE Journal*, 2017, **63**, 2248–2256.

55. W. Silva, M. Zanatta, A. S. Ferreira, M. C. Corvo and E. J. Cabrita, *IJMS*, 2020, **21**, 7745.

56. J. A. Widegren, E. M. Saurer, K. N. Marsh and J. W. Magee, *The Journal of Chemical Thermodynamics*, 2005, **37**, 569–575.

57. C. A. Tibbetts, A. B. Wyatt, B. M. Luther, A. K. Rappé and A. T. Krummel, *J. Phys. Chem. B*, 2023, **127**, 932–943.

58. A. M. O'Mahony, D. S. Silvester, L. Aldous, C. Hardacre and R. G. Compton, *J. Chem. Eng. Data*, 2008, **53**, 2884–2891.

59. C. D. Tran, S. H. De Paoli Lacerda and D. Oliveira, *Appl Spectrosc*, 2003, **57**, 152–157.

60. K. Mukherjee, S. Palchowdhury and M. Maroncelli, *J. Phys. Chem. B*, 2024, **128**, 3689–3706.

61. S. Palchowdhury, K. Mukherjee and M. Maroncelli, *The Journal of Chemical Physics*, 2022, **157**, 084502.

62. J. D. Cyran and A. T. Krummel, *The Journal of Chemical Physics*, 2015, **142**, 212435.

63. J. D. Cyran, J. M. Nite and A. T. Krummel, *J. Phys. Chem. B*, 2015, **119**, 8917–8925.

64.M.J. Frisch, G.W. Trucks, H.B. Schlegel, G.E. Scuseria, M.A. Robb, J.R. Cheeseman, G. Scalmani, V. Barone, G.A. Petersson, H. Nakatsuji, X. Li, M. Caricato, A.V. Marenich, J. Bloino, B.G. Janesko, R. Gomperts, B. Mennucci, H.P. Hratchian, J.V. Ortiz, A.F. Izmaylov, J.L. Sonnenberg, Williams, F. Ding, F. Lipparini, F. Egidi, J. Goings, B. Peng, A. Petrone, T. Henderson, D. Ranasinghe, V.G. Zakrzewski, J. Gao, N. Rega, G. Zheng, W. Liang, M. Hada, M.

Ehara, K. Toyota, R. Fukuda, J. Hasegawa, M. Ishida, T. Nakajima, Y. Honda, O. Kitao, H. Nakai, T. Vreven, K. Throssell, J.A. Montgomery Jr., J.E. Peralta, F. Ogliaro, M.J. Bearpark, J.J. Heyd, E. N. Brothers, K.N. Kudin, V.N. Staroverov, T.A. Keith, R. Kobayashi, J. Normand, K. Raghavachari, A.P. Rendell, J.C. Burant, S.S. Iyengar, J. Tomasi, M. Cossi, J.M. Millam, M. Klene, C. Adamo, R. Cammi, J.W. Ochterski, R.L. Martin, K. Morokuma, O. Farkas, J.B. Foresman, D.J. Fox, Gaussian 16 Rev. C.01, in, Wallingford, CT, 2016.

.

65. H. M. A. Rahman and R. Buchner, *Journal of Molecular Liquids*, 2012, **176**, 93–100.

66. K. Mukherjee, S. Palchowdhury and M. Maroncelli, *J. Phys. Chem. B*, 2022, **126**, 4584–4598.

67. M. I. Cabaço, M. Besnard, Y. Danten and J. A. P. Coutinho, *J. Phys. Chem. B*, 2011, **115**, 3538–3550.

68. J. S. Rao, T. C. Dinadayalane, J. Leszczynski and G. N. Sastry, *J. Phys. Chem. A*, 2008, **112**, 12944–12953.

69. K. Fujii, M. Sogawa, N. Yoshimoto and M. Morita, *J. Phys. Chem. B*, 2018, **122**, 8712–8717.

70. N. Deora and P. R. Carlier, *J. Org. Chem.*, 2010, **75**, 1061–1069.

71. N. R. Dhumal, H. J. Kim and J. Kiefer, *J. Phys. Chem. A*, 2009, **113**, 10397–10404.

72. D. G. Kuroda, D. Yu. Vorobyev and R. M. Hochstrasser, *The Journal of Chemical Physics*, 2010, **132**, 044501.

73. S. Lotze and H. J. Bakker, *The Journal of Chemical Physics*, 2015, **142**, 212436.

74. T. Elsaesser, N. Huse, J. Dreyer, J. R. Dwyer, K. Heyne and E. T. J. Nibbering, *Chemical Physics*, 2007, **341**, 175–188.

75. P. Yee, J. K. Shah and E. J. Maginn, *J. Phys. Chem. B*, 2013, **117**, 12556–12566.

76. L. Zhang, Z. Xu, Y. Wang and H. Li, *J. Phys. Chem. B*, 2008, **112**, 6411–6419.

77. Y. Chen, S. Li, Z. Xue, M. Hao and T. Mu, *Journal of Molecular Structure*, 2015, **1079**, 120–129.

78. V. Gutmann, *Coordination Chemistry Reviews*, 1976, **18**, 225–255.

79. A. Regis and J. Corset, *Chemical Physics Letters*, 1975, **32**, 462–465.

80. E. Spinner, *J. Chem. Soc.*, 1964, 4217.

81. K. O. Christe and D. Naumann, *Spectrochimica Acta Part A: Molecular Spectroscopy*, 1973, **29**, 2017–2024.

82. D. T. Bowron, C. D'Agostino, L. F. Gladden, C. Hardacre, J. D. Holbrey, M. C. Lagunas, J. McGregor, M. D. Mantle, C. L. Mullan and T. G. A. Youngs, *J. Phys. Chem. B*, 2010, **114**, 7760–7768.

83. Y.-J. Lin, N. Hossain and C.-C. Chen, *Journal of Molecular Liquids*, 2021, **329**, 115524.

84. S. Cha, M. Ao, W. Sung, B. Moon, B. Ahlström, P. Johansson, Y. Ouchi and D. Kim, *Phys. Chem. Chem. Phys.*, 2014, **16**, 9591–9601.

85. N. H. C. Lewis, B. Dereka, Y. Zhang, E. J. Maginn and A. Tokmakoff, *J. Phys. Chem. B*, 2022, **126**, 5305–5319.

86. M. Pastorczak, K. Duk, S. Shahab and A. A. Kananenka, *J. Phys. Chem. B*, 2023, **127**, 4843–4857.

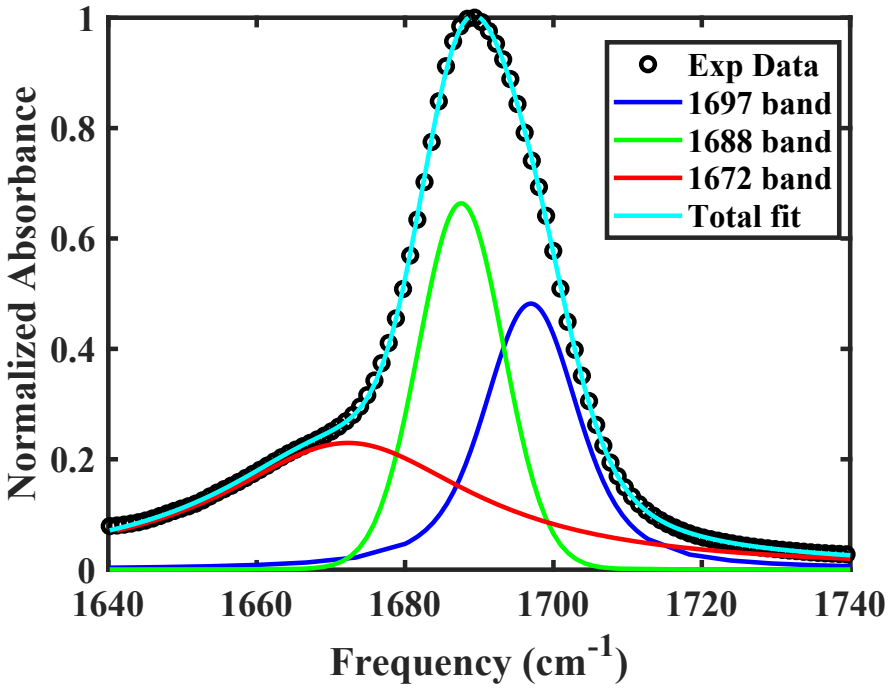

Figure 1/Mukherjee et al

Figure 1. Asymmetric carboxylate stretching band of neat Emim:TFA (black open circles) and corresponding multi-Voigt fit are shown in solid lines. Here (and in later figures) absorbance is shown normalized to unity.

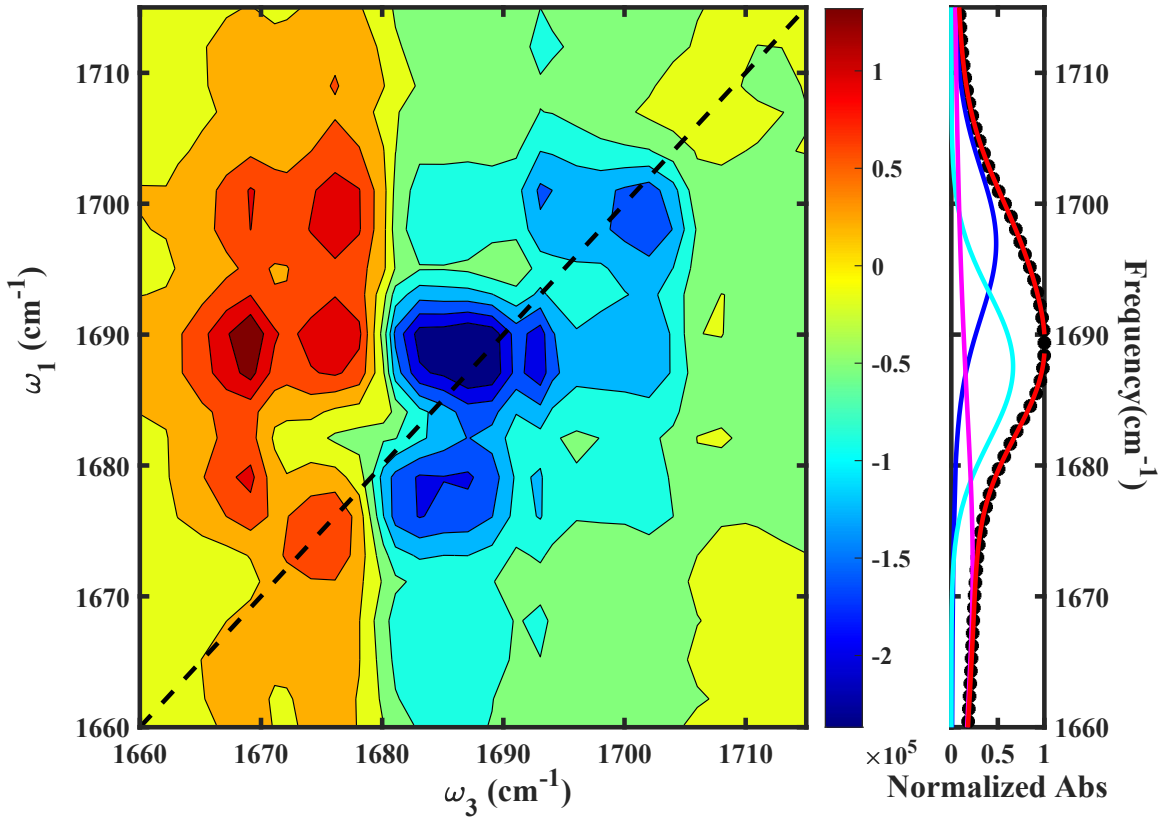

Figure 2/Mukherjee et al

Figure 2. Comparison of the 2DIR spectra (in the co-polarized geometry) to the deconvoluted linear spectrum of neat Emim:TFA. ω_1 and ω_3 depict the pump and probe axes, respectively.

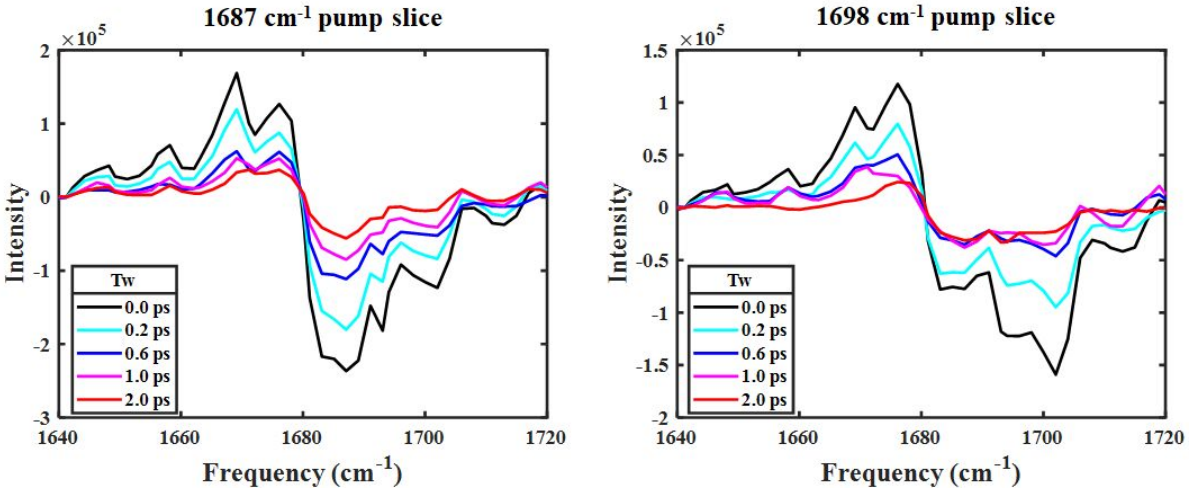

Figure 3/Mukherjee et al

Figure 3. Pump slices along ω_1=1694 cm^{-1} (A) and ω_1=1704 cm^{-1} (B) from the co-polarized 2DIR spectra of neat Emim:TFA at different T_w values.

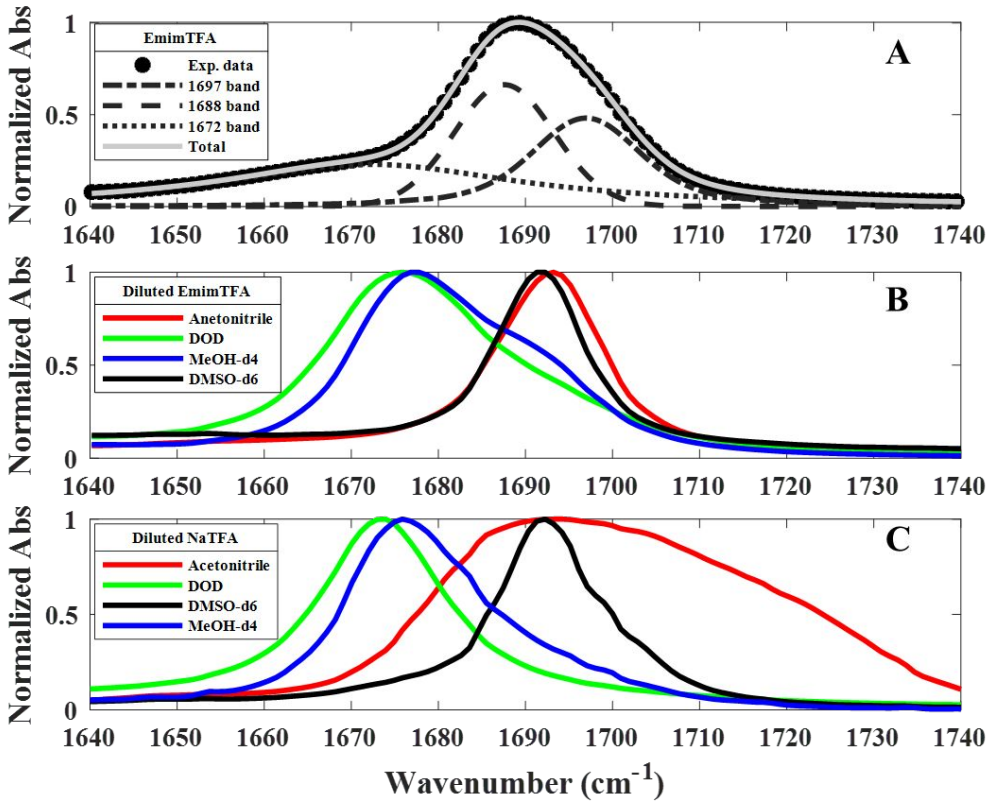

Figure 4/Mukherjee et al

Figure 4. Linear spectra of the TFA asymmetric carboxylate stretching band in undoped Emim:TFA (A), diluted Emim:TFA (B) and NaTFA (C) in the solvents D_2O (green), deuterated methanol (blue), acetonitrile (red), and deuterated DMSO (black).

C2H….TFA

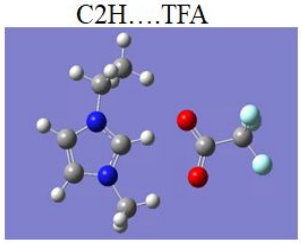

Mode	Frequency(cm^{-1})	Intensity
C=O asy str. (ε = 27)	1701	924

C4/5H….TFA

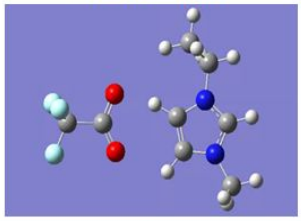

Mode	Frequency(cm^{-1})	Intensity
C=O asy str. (ε = 27)	1704	902

Ion Pair

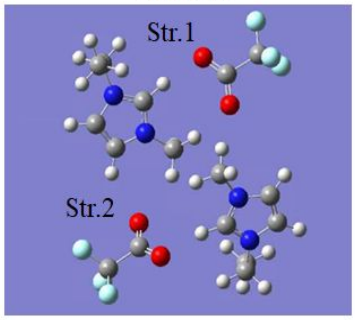

Mode	Frequency(cm^{-1})	Intensity
C=O asy str. 1 (ε = 27)	1701	846
C=O asy str. 2 (ε = 27)	1704	1254

Figure 5/Mukherjee et al

Figure 5. Optimized structures of two single ion pairs (left panel) and a double ion pair (right panel). The tables under each figure provide the calculated frequencies and intensities of the TFA^- asymmetric carboxylate stretch in these structures. The dielectric constant used for the implicit solvent in these calculations are given in the parentheses.

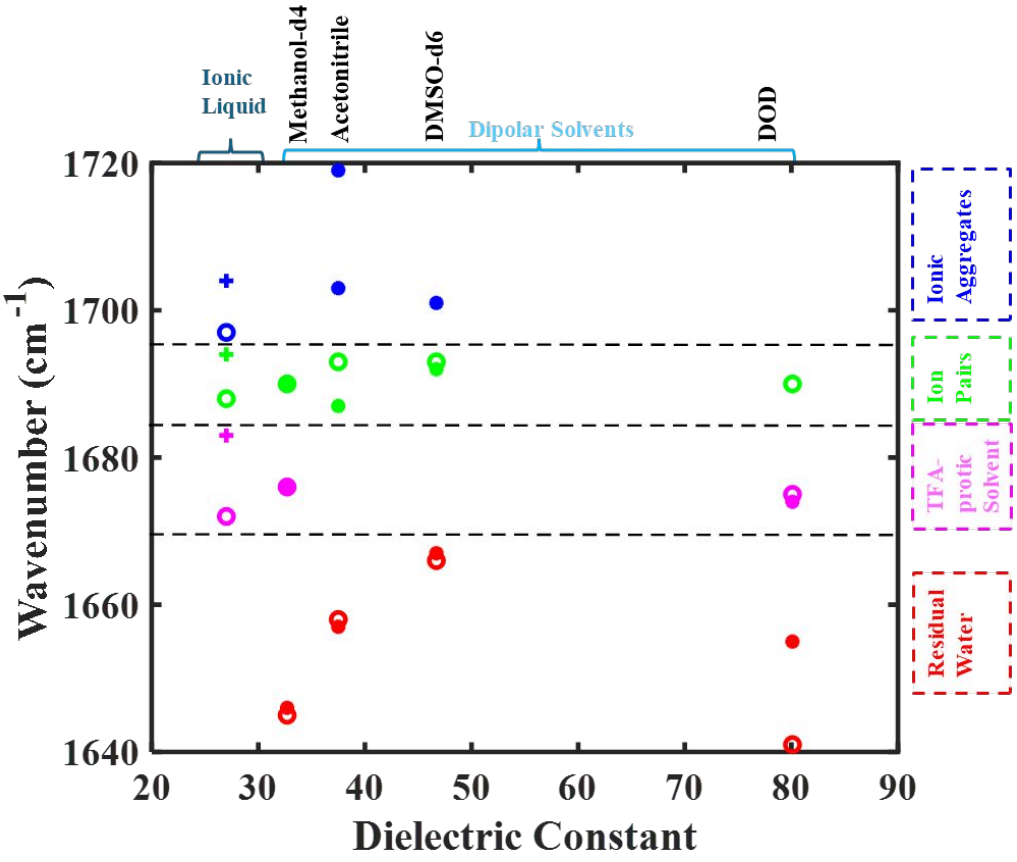

Figure 6/Mukherjee et al

Figure 6. Peak frequencies of the fit components of the asymmetric carboxylate stretching band of TFA anion of NaTFA (squares) and Emim:TFA (circles) in different solvents. Assignments are denoted by color. Solvents are organized according to dielectric constant. For completeness the diagonal peak frequencies of the 2DIR spectrum of neat Emim:TFA are marked with + symbols.

Data Availability: The data supporting this article have been included as part of the Supplementary Information.